

# The Impact of Primordial Magnetic Fields on Future CMB Bounds on Inflationary Gravitational Waves.

Fabrizio Renzi,<sup>1,\*</sup> Giovanni Cabass,<sup>2,†</sup> Eleonora Di Valentino,<sup>3,‡</sup> Alessandro Melchiorri,<sup>1,§</sup> and Luca Pagano<sup>4,5,6,¶</sup>

<sup>1</sup>*Physics Department and INFN, Università di Roma “La Sapienza”, Ple Aldo Moro 2, 00185, Rome, Italy*

<sup>2</sup>*Max-Planck-Institut für Astrophysik, Karl-Schwarzschild-Str. 1, 85741 Garching, Germany*

<sup>3</sup>*Jodrell Bank Center for Astrophysics, School of Physics and Astronomy,  
University of Manchester, Oxford Road, Manchester, M13 9PL, UK*

<sup>4</sup>*Institut d’Astrophysique Spatiale, CNRS, Univ. Paris-Sud,  
Université Paris-Saclay, Bât. 121, 91405 Orsay cedex, France*

<sup>5</sup>*Institut d’Astrophysique de Paris, CNRS, 98 bis Boulevard Arago, F-75014, Paris, France*

<sup>6</sup>*LERMA, CNRS, Observatoire de Paris, 61 Avenue de l’Observatoire, Paris, France*

(Dated: December 3, 2024)

We discuss whether an unaccounted contribution to the Cosmic Microwave Background polarization  $B$ -mode by primordial magnetic fields (PMFs) can bias future constraints on inflationary gravitational waves. As a case-study, we consider a PMF amplitude of  $\approx 1$  nG on 1 Mpc scales, compatible with current cosmological bounds. We find a degeneracy in the  $B$ -mode spectra between PMFs and inflationary GWs. If PMFs of this amplitude are not accounted for, future CMB experiments could claim a false detection of a tensor/scalar ratio  $r \approx 0.007$ , close to the predictions of Starobinsky and  $\alpha$ -attractor models. The degeneracy can be broken if  $B$ -modes are measured also at multipoles  $\ell \gtrsim 900$ : more precisely experiments like CMB-S4 or CORE-M5 would be able to discriminate PMFs from primordial GWs at high statistical significance. Experiments as LiteBIRD or PIXIE will not be able to break the degeneracy and will need complementary bounds coming, for example, from measurements of anisotropies in the Faraday rotation angle of CMB polarization. This reinforces the importance of future experimental constraints on PMFs.

## I. INTRODUCTION

One of the main goals of modern cosmology is the detection of Cosmic Microwave Background polarization  $B$ -modes produced by inflationary gravitational waves. Their detection will not only provide a “smoking gun” for the inflationary paradigm but will also determine several fundamental properties of the inflationary model itself. In particular, for slow-roll inflation, a detection of these primordial GWs would shed light not only on the energy scale of inflation but also provide key information on the first two derivatives of the inflaton potential, opening a window on physics at extremely high energies (see e.g. [1–4] for recent reviews).

In the past years the experimental bounds on the primordial  $B$ -mode component (parameterized by the tensor-to-scalar ratio  $r$ ) have improved significantly. Indeed, since the constraints from the BICEP experiment of  $r < 0.72$  at 95% C.L. [5] in 2010, the recent combined analysis of BICEP2, Keck Array IV and Planck  $B$ -mode measurements now provide  $r < 0.07$  at 95% C.L. [6], showing an improvement by nearly one order of magnitude in about  $\sim 7$  years (see also [7]). In the next years a further improvement by one order of magnitude, reaching a sensitivity in the range of  $r \sim 10^{-2} - 10^{-3}$ , is expected

by several ongoing experiments such as BICEP3 and the Keck Array [8], CLASS [9], Advanced ACTPol [10], and SPT-3G [11]. Future experiments as the LiteBIRD [12] and CORE-M5 [13–15] satellite missions and the CMB-S4 ground based telescope [16] are expected to reach a sensitivity of  $\delta r \sim 0.0001$ .

This ambitious experimental program will clearly provide key information on the physics of inflation. It is however important to investigate if different physical mechanisms than primordial gravitational waves could generate a  $B$ -mode polarization signal that could lead to a wrong claim for detection. Foregrounds as galactic dust are obviously an issue for a reliable detection of primordial  $B$ -modes but multi-frequency measurements should be able to fully address their impact (see e.g. [17, 18]). Topological defects (see e.g. [19]) can also produce  $B$ -modes (even from vector perturbations [20]), however the shape of the angular spectrum is in this case very different and accurate measurements should differentiate between the two generation mechanisms.

Another possible physical mechanism able to produce  $B$ -mode polarization and that could mimic primordial gravitational waves are magnetic fields (see e.g. [21]). In the presence of primordial magnetic fields (PMFs), passive tensor modes and compensated vector modes can indeed produce  $B$ -modes with angular spectra that are very similar in shape to those produced by primordial gravitational waves and lensing (see e.g. [22–25]). Future CMB experiments like CMB-S4 will be extremely sensitive to primordial magnetic fields, improving current constraints on the corresponding  $B$ -mode amplitude by nearly two orders of magnitude [27].

---

\* [fabrizio.renzi@uniroma1.it](mailto:fabrizio.renzi@uniroma1.it)

† [gcabass@mpa-garching.mpg.de](mailto:gcabass@mpa-garching.mpg.de)

‡ [eleonora.divalentino@manchester.ac.uk](mailto:eleonora.divalentino@manchester.ac.uk)

§ [alessandro.melchiorri@roma1.infn.it](mailto:alessandro.melchiorri@roma1.infn.it)

¶ [lpagano@ias.u-psud.fr](mailto:lpagano@ias.u-psud.fr)

Since magnetic fields are essentially ubiquitous in astrophysics with evidence also on cosmological scales (see [28] for a review) and since the possibility of a production in the early universe is certainly plausible, it is extremely timely to investigate how well future CMB experiments could discriminate between gravitational waves and primordial magnetic fields in the generation of CMB polarization  $B$ -modes.

One key difference is that while gravitational waves decay inside the horizon and affect the CMB anisotropies on large angular scales, primordial magnetic fields affect also smaller angular scales through compensated perturbations (see e.g. [25, 29]). As we show later in this paper, CMB experiments sensitive mainly to large angular scales as the proposed PIXIE and LiteBIRD mission are essentially unable to discriminate between GWs and PMFs. A clear and reliable detection of  $B$ -modes generated by gravitational waves can be obtained only by considering also smaller scales as planned by the CMB-S4 experiments or by a satellite with improved angular resolution as the recent CORE-M5 proposal.

PMFs can be constrained also by measuring the Faraday rotation of CMB polarization (see e.g. [29] and references therein). It is therefore important to evaluate the complementary experimental bounds that can be achieved from future experiments.

Our paper is structured as follows: in Section II we briefly review the physics behind the formation of CMB anisotropies and polarization from primordial magnetic fields. In Section III we discuss our forecast method while in Section IV we present our results. We discuss the constraints from Faraday rotation in Section V. We finally conclude in Section VI.

## II. PRIMORDIAL MAGNETIC FIELDS

In this section we discuss the main features of primordial magnetic fields following [22–24, 28, 30]. We consider a stochastic magnetic field  $B^i(x^j, \eta)$  generated by some mechanism at a time  $\eta_B$  before the epoch of neutrino decoupling  $\eta_\nu$ . The very early universe is filled with a highly ionized plasma with an extremely high conductivity: this allows us to take the ideal magnetohydrodynamic (MHD) limit of Maxwell's equations, an approximation which is rigorously valid during radiation dominance [31]. In general, the electromagnetic field sources both an energy flux and an anisotropic shear so, to maintain the homogeneity and isotropy of a FRW cosmology, one must ensure that these vanish on the background. On the one hand, removing electromagnetic shear from the background cosmology (that we assume to be spatially flat) leads to neglecting many possibly interesting effects of PMF on cosmological fluids, e.g. the direct sourcing of tensor perturbations or gravity back-reaction on the PMF, and most of the MHD structure is removed. However, it allows to reduce Maxwell's equations in a Friedmann-Robertson-Walker metric to the form they have in flat spacetime if

the electromagnetic fields are replaced by their co-moving counterpart, see e.g. Appendix B of [28]. With all these approximations the magnetic flux is conserved. Then, the field is frozen in the plasma and satisfies

$$\frac{\partial}{\partial \eta} (a^2 B^i(x^j, \eta)) = 0. \quad (1)$$

Here  $a = a(\eta)$  is the scale factor at some conformal time  $\eta$  normalized so that  $a(\eta_0) = 1$  at the present conformal time  $\eta_0$ . Thus the co-moving magnetic field is time-independent while the physical field has amplitude scaling as  $a^{-2}$ , i.e.  $B^i(x^j, \eta) = B^i(x^j)/a^2$ . Since in the MHD limit the electric field is vanishing, the perturbed stress-energy tensor of the magnetic field can be written as

$$\delta T_0^0 = -\frac{1}{8\pi a^4} B^2(\mathbf{x}) \quad (2)$$

$$= -\rho_\gamma \Delta_B,$$

$$\delta T_j^i = \frac{1}{4\pi a^4} \left( \frac{1}{2} B^2(\mathbf{x}) \delta_j^i - B^i(\mathbf{x}) B_j(\mathbf{x}) \right) \quad (3)$$

$$= p_\gamma (\Delta_B \delta_j^i + (\Pi_B)_j^i),$$

where  $\rho_\gamma$  and  $p_\gamma = \rho_\gamma/3$  are the photon density and pressure and are included to account for factors of  $a^{-4}$ , while  $\Delta_B$  and  $(\Pi_B)_j^i$  are the magnetic contributions to the radiation density contrast and the dimensionless anisotropic stress respectively. In deriving Eqs. (2), (3) the background magnetic field is assumed to vanish: so, the unperturbed stress-energy tensor is the same as without a PMF.

### A. Magnetically-induced Modes

The main difference with the standard theory of CMB anisotropies introduced by the presence of a magnetic field in the early universe is to modify the perturbed stress-energy tensor with the addition of two terms,  $\Delta_B$  and  $(\Pi_B)_j^i$ , that corresponds to magnetic pressure and tension of non-relativistic MHD. Depending on the generation epoch of the PMF three different class of magnetic perturbations can be distinguished: inflationary, passive and compensated. As shown in [32], inflationary modes are sourced by the effect of magnetic stress on curvature during inflation and leads to a constant contribution to the curvature perturbation. However, it is important to notice that mechanisms that produce sizable magnetic fields on super-horizon scales during inflation often lead to strong production of electric fields, and with them to back-reaction effects and strong coupling between the inflaton and the magnetic field [33, 34]. Moreover, due to Schwinger pair production, these electric fields can induce sufficiently large conductivity to terminate the phase of magnetogenesis [35].<sup>1</sup> Therefore,

<sup>1</sup> Also post-inflationary (i.e. between inflation and reheating) magnetogenesis has been considered in the literature: however, it is

the features of such magnetic inflationary modes strongly depends on the generation mechanism and are here neglected to maintain generality. In the rest of the paper we will focus only on passive and compensated mode which are sourced by every PMF independently of the magnetic generation history. Passive modes are generated before neutrino decoupling ( $\eta < \eta_\nu$ ) since, without neutrino free-streaming, there is no counterpart in the photon-baryon fluid able to compensate for the PMF anisotropic stress, which therefore sources both adiabatic scalar and tensor perturbations [22–24, 36]. When neutrinos decouple ( $\eta \geq \eta_\nu$ ) from photons, they also produce an anisotropic stress that compensates the magnetic one leading to isocurvature-like perturbations, the so-called compensated modes [22–24, 36, 37].

The amplitude of these modes is set by the comoving curvature perturbation  $\zeta$ . In standard cosmology  $\zeta$  is conserved on super-horizon scales, but the presence of a PMF sources the growth of  $\zeta$  before neutrino decoupling through the anisotropic stress  $\Pi_B$  [24]. Once neutrino compensation on the PMF anisotropic stress is effective, the growth of  $\zeta$  ceases. For scalar perturbations the final form of  $\zeta$  is

$$\zeta \approx \zeta(\eta_B) - \frac{1}{3} R_\gamma \Pi_B \left[ \ln(\eta_\nu/\eta_B) + \left( \frac{5}{8R_\nu} - 1 \right) \right], \quad (4)$$

where  $\zeta(\eta_B)$  is the comoving perturbation at the time of PMF generation and contains all the information regarding perturbations produced before  $\eta_B$ , and  $R_i$  represents the ratio between the total density and the density of the species  $i$ . From Eq. (4) we see that there are two main contributions to  $\zeta$ . The first contribution which has amplitude proportional to the product  $\Pi_B \ln(\eta_\nu/\eta_B)$  comes from the passive modes and is an adiabatic-like perturbation but with non-Gaussian statistics. These modes grow logarithmically in time when  $\eta_B \leq \eta \leq \eta_\nu$  and then evolve passively after neutrino decoupling. For an unknown generation mechanism the exact time and details of magnetic field production cannot be clearly defined. As an illustration we will allow  $\eta_\nu/\eta_B$  to range from  $10^6 - 10^{12}$  [24]. As it will be shown, the variation over  $\eta_\nu/\eta_B$  is useful to test the degeneracy in the amplitude of the passive mode spectrum (see section IV). The other contribution instead is the contribution of the compensated mode proportional to  $\Pi_B$  but having also a dependency from  $\Delta_B$  in the ratio  $R_\gamma/R_\nu$ . These are isocurvature-like modes sourced by the residual  $\Pi$  after neutrino compensation and magnetic energy density. An expression similar to Eq.(4) can be derived for tensor perturbations which come from both the passive and compensated modes, with  $\Pi_B$  replaced by  $\Pi_B^{(T)}$ . However

compensated tensor modes have amplitudes so small that can be safely neglected [36]. Since vector perturbations rapidly decays when not continuously sourced, there are no passive vector mode, but again the compensated mode is proportional to  $\Pi_B^{(V)}$ .

## B. Statistics and Power Spectra of PMFs

We model magnetic field statistics on the assumption that PMFs are a statistically isotropic Gaussian field with no helicity, i.e. helical fields are not included in our analysis (a review on the impact of helical field on CMB can be found in [30]). The corresponding two-point correlation function in the Fourier space is then written as

$$\langle B_i(\mathbf{k}) B_j^*(\mathbf{k}') \rangle = (2\pi)^3 \delta^{(3)}(\mathbf{k} - \mathbf{k}') P_{ij}(\hat{\mathbf{k}}) P_B(k), \quad (5)$$

where the projector  $P_{ij} = \delta_{ij} - \hat{k}_i \hat{k}_j$  comes from the fact that the magnetic field is a solenoidal vector field. The exact form of the power spectrum  $P_B$  strongly depends on the mechanism generating the PMF. We choose to follow the current literature defining  $P_B$  as a simple power law with a cut-off scale  $k_D$ , i.e.

$$P_B(k) = \begin{cases} \mathcal{A} k^{n_B} & k < k_D, \\ 0 & \text{otherwise.} \end{cases} \quad (6)$$

The spectral index  $n_B$  depends on the details of PMF generation. For instance, inflationary magnetogenesis favors a red-tilted spectrum ( $n_B \leq 0$ ), while magnetic fields produced during, e.g., the electroweak phase transition have blue-tilted spectra with  $n_B \geq 2$ .<sup>2</sup> We will focus only on nearly scale-invariant spectra ( $n_B$ ) since they are dominated by tensor passive modes (i.e. most of their power is concentrated at very large scales), and we are interested in the degeneracy that could possibly arise with inflationary tensor modes at high  $\ell$ . Note that an increase of  $n_B = -2.9$  towards bluer spectra only makes power shift from large to small scales resulting in a reduction of the amplitude of tensor passive modes. The scale  $k_D$ , instead, accounts for the damping of the magnetic field due to radiation viscosity on very small scales, where magnetic effects are suppressed by photon diffusion. This scale is of order the comoving Silk damping scale times the dimensionless Alfvén velocity. We define

<sup>2</sup> PMFs with very blue spectra are strongly constrained by CMB data [25, 38, 39]. In [25] an upper limit of  $B_{1 \text{ Mpc}} < 0.002 \text{ nG}$  at 95% C.L. for models with  $n_B = 2$  has been recently found. Similarly, very strong constraints can be imposed for PMFs produced during inflation with  $n_B \sim 0$ , see e.g. [26]. Constraints remain elusive, instead, for nearly scale-invariant PMFs (i.e.  $n_B \gtrsim -3$ ). For a detailed discussion on the PMF generation history see [28, 30].

worth stressing that also in this case one can run into back-reaction or strong-coupling problems, implying that successful models must have an extremely low reheating temperature, possibly spoiling bounds from Big Bang Nucleosynthesis [33].

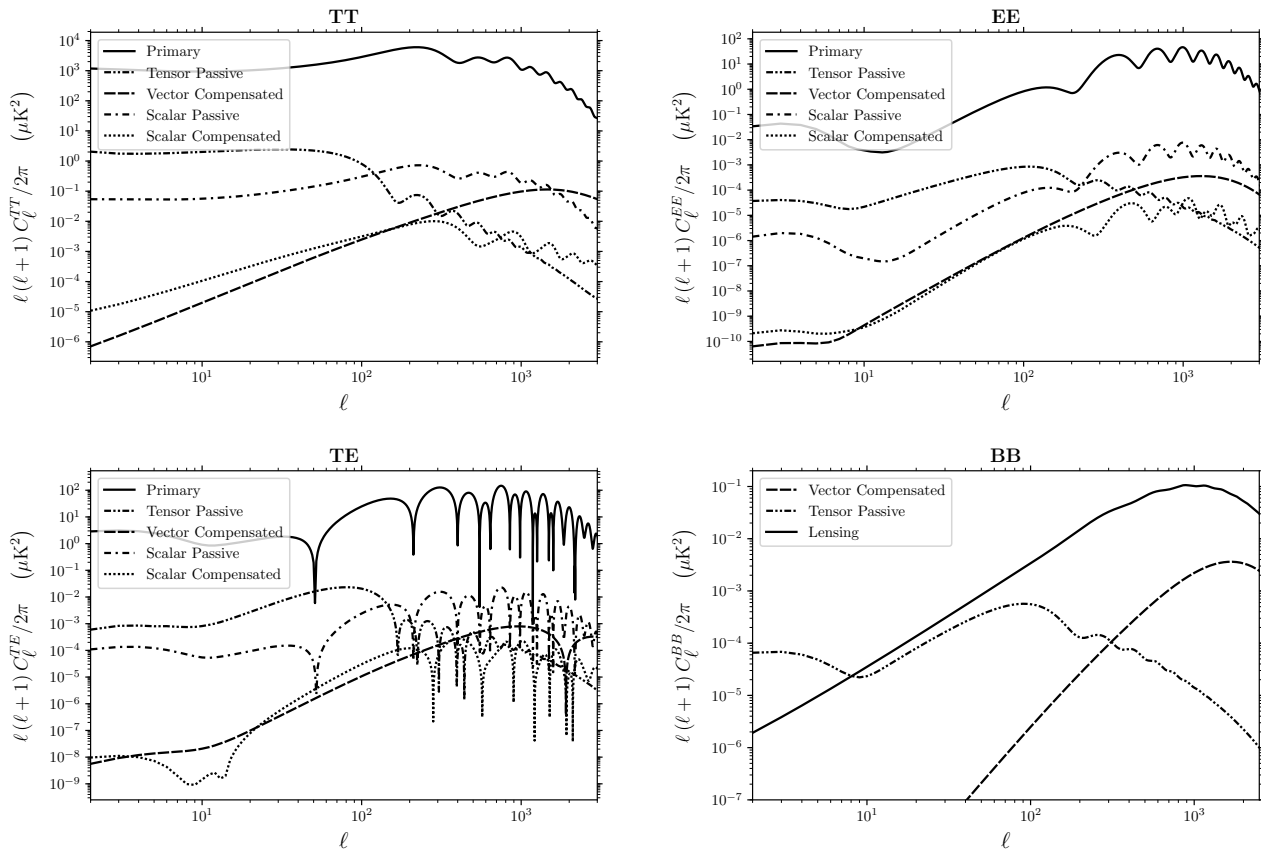


Figure 1. Comparison between primary and magnetic contributions to CMB angular correlation functions computed with MAGCAMB [25]. As values for parameters we take:  $\Omega_b h^2 = 0.02225$ ,  $\Omega_c h^2 = 0.1198$ ,  $\tau = 0.055$ ,  $100\theta_{\text{MC}} = 1.04077$ ,  $\ln(10^{10} A_s) = 3.094$ ,  $n_s = 0.9645$ ,  $B_{1\text{Mpc}} = 1.08\text{ nG}$ ,  $\eta_\nu/\eta_B = 10^{12}$ ,  $n_B = -2.9$  (these are the same values of Table II, i.e. the fiducial model for our forecasts). The most important magnetic contribution to CMB angular spectra is in the B-mode polarization at large scales ( $\ell \lesssim 100$ ) where the magnetic tensor mode is greater than or comparable with lensing.

such scale according to [40, 41], i.e.

$$\frac{k_D}{\text{Mpc}^{-1}} = \left[ 5.5 \times 10^4 h \left( \frac{B_\lambda}{\text{nG}} \right)^{-2} \times \left( \frac{2\pi}{\lambda/\text{Mpc}} \right)^{n_B+3} \frac{\Omega_b h^2}{0.022} \right]^{\frac{1}{n_B+5}}, \quad (7)$$

as usual,  $\Omega_b$  and  $h$  are the baryon density fraction and the reduced Hubble constant. Regarding the magnetic field amplitude, we follow the current literature and describe it in terms of  $B_\lambda$ , obtained smoothing the magnetic energy density with a Gaussian filter over a comoving scale  $\lambda$ , that is

$$B_\lambda^2 = \frac{\mathcal{A}}{2\pi^2} \frac{\Gamma(\frac{n_B+3}{2})}{\lambda^{n_B+3}}. \quad (8)$$

In the following, we will take  $\lambda = 1\text{ Mpc}$ , this value of  $\lambda$  is justified by the fact that the observed magnetic fields are tangled (coherent) on scales of order of the typical size of a cluster, i.e.  $\sim \text{few Mpc}$ . In Fig. 1 we report the components of the magnetic power spectrum corresponding to the values of our fiducial model (Tab. II).

For this set of parameters, PMFs have a significant effect on CMB angular spectra only in the polarization power spectrum for  $\ell \leq 100$ . With this realization we expect that PMFs would be constrained only through B-mode polarization spectrum, where they dominate at very large scales. Such features will allow us to understand how efficiently the magnetic field would be constrained throughout the BB spectrum. This signature in the CMB spectra is sourced by magnetic tensor perturbations i.e. gravity waves. Their imprint at large scales is completely equivalent to that expected from inflationary gravitational waves. Therefore a degeneracy between the amplitude of these modes arises. However magnetic vector perturbations imprint B-modes spectrum at very small scales: a features not shared by inflationary tensor modes (see Fig.2). We will show in the following that this degeneracy could be solved measuring the small scale features of the magnetic spectrum and also that CMB probes able to measure both small and large scales like a CORE-like satellite or CMB-S4 will resolve such degeneracy.

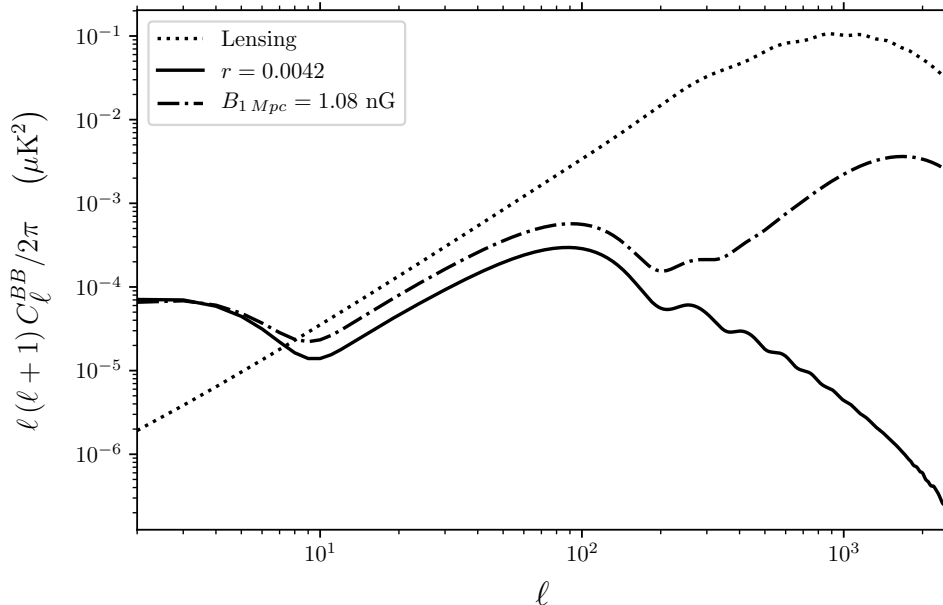


Figure 2. Comparison between the  $B$ -mode angular power spectra for  $B_{1\text{ Mpc}} = 1.08\text{ nG}$  and  $r = 0.0042$ . The CMB spectra have been computed with MAGCAMB [25]. In this particular case, the superimposition between the inflationary and magnetic tensor modes is realized at very large scales where both contributions are about two order of magnitude over lensing spectrum.

### III. METHOD

In this section we briefly illustrate the method we adopted to derive our forecasts for future CMB experiments.

We follow the same procedure (now standard practice) used in [42]. We produce synthetic realizations of future data given by

$$\hat{C}_\ell = C_\ell|_{\text{fid}} + N_\ell. \quad (9)$$

On the right-hand side, the  $C_\ell|_{\text{fid}}$  are the angular power spectra of the fiducial model in  $\mu\text{K}^2$  and

$$N_\ell = w^{-1} \exp(\ell(\ell+1)\theta^2/8 \ln 2) \quad (10)$$

gives the experimental noise, where  $w^{-1/2}$  is the experimental power noise expressed in  $\mu\text{K} \cdot \text{rad}$  and  $\theta$  is the experimental FWHM angular resolution in radians (we assume that pixel noise is uniform and uncorrelated). We have considered several future experiments with technical specifications listed in Tab. I. More specifically we consider the PIXIE [43], LiteBIRD [12] and CORE-M5 [15] satellite missions, and the Stage-3 (see e.g. [44]) and CMB-S4 [16] ground-based experiments<sup>3</sup>. The simulated

data are then compared with theoretical  $C_\ell$  obtained from the publicly available code MAGCAMB<sup>4</sup> [25], based on a modified version of the Boltzmann integrator CAMB [45]. Given a theoretical model, its likelihood  $\mathcal{L}$  is given by:

$$-2 \ln \mathcal{L} = \sum_\ell (2\ell+1) f_{\text{sky}} \left( \frac{D}{|\bar{C}|} + \ln \frac{|\bar{C}|}{|\hat{C}|} - 3 \right), \quad (11)$$

where  $\hat{C}_\ell$  are the fiducial spectra plus noise of Eq. 9,  $\bar{C}_\ell$  are the theory spectra plus noise, and  $f_{\text{sky}}$  is the sky fraction observed by the experiment. Moreover,  $|\bar{C}|$ ,  $|\hat{C}|$  are given by:

$$|\bar{C}| = \bar{C}_\ell^{TT} \bar{C}_\ell^{EE} \bar{C}_\ell^{BB} - (\bar{C}_\ell^{TE})^2 \bar{C}_\ell^{BB}, \quad (12)$$

$$|\hat{C}| = \hat{C}_\ell^{TT} \hat{C}_\ell^{EE} \hat{C}_\ell^{BB} - (\hat{C}_\ell^{TE})^2 \hat{C}_\ell^{BB}, \quad (13)$$

while  $D$  is

$$D = \hat{C}_\ell^{TT} \bar{C}_\ell^{EE} \bar{C}_\ell^{BB} + \bar{C}_\ell^{TT} \hat{C}_\ell^{EE} \bar{C}_\ell^{BB} + \bar{C}_\ell^{TT} \bar{C}_\ell^{EE} \hat{C}_\ell^{BB} - \bar{C}_\ell^{TE} \left( \bar{C}_\ell^{TE} \hat{C}_\ell^{BB} + 2 \hat{C}_\ell^{TE} \bar{C}_\ell^{BB} \right). \quad (14)$$

In the following, we sample the likelihood of Eq. (11) using a MAGCAMB-compatible [25] version of the Monte Carlo Markov Chain code CosmoMC<sup>5</sup> [46], based on the

<sup>3</sup> Most of these experiments are still in the stage of a proposal. The above list should therefore be considered as an illustration of what a future CMB experiments could achieve.

<sup>4</sup> <https://alexzucca90.github.io/MagCAMB/>

<sup>5</sup> <http://cosmologist.info>

Metropolis-Hastings algorithm with chains convergence tested by the Gelman and Rubin method. Since we assumed no correlation between primary adiabatic and magnetic modes, both theory and fiducial  $C_\ell$  are obtained simply adding linearly together magnetic and non-magnetic contributions, i.e.

$$C_\ell = C_\ell^{\text{primary}} + C_\ell^{\text{passive}} + C_\ell^{\text{compensated}}. \quad (15)$$

As fiducial model, we assume a flat  $\Lambda$ CDM model with parameters compatible with the recent Planck 2015 constraints [39, 47, 48], as listed in Tab. II. The fiducial magnetic field amplitude, compatible with current bounds from Planck [39], is  $B_{1\text{Mpc}} = 1.08\text{ nG}$ . It gives a  $B$ -mode power spectrum similar to the one corresponding to  $r = 0.0042$ , i.e. the prediction of the Starobinsky  $R^2$  model [49] for  $N_\star \approx 53$  ( $N_\star$  being the number of  $e$ -folds of the observable part of the inflationary epoch): we show this in Fig. 2. We take, then, this value of  $B_{1\text{Mpc}}$  as a case-study, using it to show how an unresolved PMF component can bias the constraints on the theoretically motivated class of inflationary models known as  $\alpha$ -attractors [50]. We also study the impact of delensing on future constraints. We subtract from the total signal the lensed CMB  $B$ -modes using the ‘‘CMB $\times$ CMB’’ delensing procedure already proposed in [51, 52]. In fact, the CMB lensing is a contaminant of the primordial  $B$ -modes, that can be estimated and partially removed from the observed signal. For each future experiment considered in this paper, we rescale the  $BB$  power spectrum by using the corresponding delensing factor [52, 53], that can be computed in the following way:

$$\alpha \equiv \frac{\sum_\ell C_\ell^{BB,\text{del}}}{\sum_\ell C_\ell^{BB,\text{len}}} \quad (16)$$

where  $C_\ell^{BB,\text{del}} \equiv C_\ell^{BB,\text{len}} - C_\ell^{BB,\text{est}}$  is the delensed  $BB$  power spectrum and  $C_\ell^{BB,\text{len}}$  is the original lensed one. The estimated lensing  $B$ -modes  $C_\ell^{BB,\text{est}}$  can be obtained by computing [51, 52]

$$C_\ell^{BB,\text{est}} = \frac{1}{2\ell+1} \sum_{\ell_1, \ell_2} |f_{\ell\ell_1\ell_2}^{EB}|^2 \times \frac{(C_{\ell_1}^{EE})^2}{C_{\ell_1}^{EE} + N_{\ell_1}^{EE}} \frac{(C_{\ell_2}^{\phi\phi})^2}{C_{\ell_2}^{\phi\phi} + N_{\ell_2}^{\phi\phi}}, \quad (17)$$

where  $f_{\ell\ell_1\ell_2}^{EB}$  is the geometric coupling factor. Finally, the estimated noise will be computed as [54]

$$N_\ell^{\phi\phi} = \left[ \frac{1}{2\ell+1} \sum_{\ell_1, \ell_2} |f_{\ell\ell_1\ell_2}^{EB}|^2 \times \frac{1}{C_{\ell_1}^{BB} + N_{\ell_1}^{BB}} \times \frac{(C_{\ell_2}^{EE})^2}{C_{\ell_2}^{EE} + N_{\ell_2}^{EE}} \right]^{-1}, \quad (18)$$

where the lensed  $B$ -modes appear. For this reason, we iterate this estimator until reaching the convergence cri-

Experiment	Beam [arcmin]	Power noise [ $\mu\text{K} \cdot \text{arcmin}$ ]	$\ell_{\text{max}}$	$\ell_{\text{min}}$	$f_{\text{sky}}$
PIXIE	96	3.0	500	2	0.7
LiteBIRD	30	3.2	3000	2	0.7
CORE-M5	3.7	2.0	3000	2	0.7
Stage-3 (Deep)	1	4	3000	50	0.06
Stage-3 (Wide)	1.4	8	3000	50	0.4
CMB-S4	3	1	3000	5	0.4

Table I. Experimental specifications for the several configurations considered in the forecasts. The power noise is defined as  $w^{-1/2} = \sqrt{4\pi\sigma^2/N}$ , where  $\sigma$  is the r.m.s. noise in each of the  $N$  pixels. We quote the power noise for temperature, and assume that for polarization it is simply enhanced by a factor of  $\sqrt{2}$ .

terion:

$$\left| \frac{N_\ell^{\phi\phi, i+1} - N_\ell^{\phi\phi, i}}{N_\ell^{\phi\phi, i+1}} \right| \leq 0.5\% . \quad (19)$$

When delensing is included in the analysis, we do not carry out a full exploration of the parameter space: we consider the likelihood of Eq. (11) for the  $BB$  angular power spectrum only, and fix all parameters apart from  $r$  and  $B_{1\text{Mpc}}$ . With these assumptions, Eq. (11) reduces to (for simplicity we drop the  $BB$  superscript on all power spectra, including noise):

$$-2 \ln \mathcal{L} = \sum_\ell (2\ell+1) f_{\text{sky}} \left[ \frac{\hat{C}_\ell}{\bar{C}_\ell} + \ln \left( \frac{\bar{C}_\ell}{\hat{C}_\ell} \right) - 1 \right], \quad (20)$$

where, following Eqs. (9, 11), we have

$$\hat{C}_\ell = C_\ell^{\text{t+PMF}}|_{\text{fid}} + \alpha \times C_\ell^{\text{lens}}|_{\text{fid}} + N_\ell, \quad (21)$$

$$\bar{C}_\ell = C_\ell^{\text{t+PMF}} + \alpha \times C_\ell^{\text{lens}} + N_\ell. \quad (22)$$

In the above equations, the ‘‘t+PMF’’ superscript labels the  $BB$  spectrum from primordial tensor modes plus the one from primordial magnetic fields (see Eq. (15)), and the ‘‘lens’’ superscript labels  $B$ -modes due to lensing. The values of the delensing parameter  $\alpha$  for the different experiments of Tab. I are collected in Tab. III.

## IV. RESULTS

### A. Results from MCMC

As discussed in the previous sections, our aim here is to investigate the impact of a PMF on the determination of the tensor-to-scalar ratio  $r$  from inflationary GWs. We therefore assume a fiducial model with no primordial GWs but with a PMF well compatible with current data. The parameters of this model are presented in Tab. II.

Parameter	Value
$\Omega_b h^2$	0.02225
$\Omega_c h^2$	0.1198
$\tau$	0.055
$n_s$	0.9645
$100 \theta_{MC}$	1.04077
$\ln(10^{10} A_s)$	3.094
$B_{1 \text{ Mpc}}$ [nG]	1.08
$\log_{10}(\eta_\nu/\eta_B)$	12
$n_B$	-2.9

Table II. Cosmological and magnetic field parameters assumed for the fiducial model.

Experiment	$\alpha$
PIXIE	1
LiteBIRD	0.94
CORE-M5	0.37
Stage-3 (Deep)	0.56
Stage-3 (Wide)	0.79
CMB-S4	0.25

Table III. Delensing factor  $\alpha$  (see Eq. (16)) for the various experiments described in Tab. I.

In what follows we analyze several simulated datasets using a modified version of CosmoMC [46], adapted to the code MAGCAMB [25] and considering a variation in the usual 6 parameters: the baryon and cold dark matter densities  $\omega_b$  and  $\omega_c$ , the amplitude and tilt of the primordial scalar spectrum of inflationary perturbations  $A_s$  and  $n_s$ , the angular size of the sound horizon at decoupling  $\theta_{MC}$ , and the optical depth at reionization  $\tau$ . In addition to these parameters, in some cases, we also include: the tensor-to-scalar ratio  $r$  computed at  $0.05 \text{ Mpc}^{-1}$ , the primordial magnetic field amplitude  $B_{1 \text{ Mpc}}$  measured in nG and the ratio between the epoch of neutrino decoupling and PMF generation,  $\eta_\nu/\eta_B$ . The inflationary tensor spectral index is given by the consistency relation  $n_t = -r/8$  while we consider only nearly scale-invariant PMFs with  $n_B = -2.9$ .

As a first step, we analyze the ability of future/planned CMB experiments (listed in Tab. I) of recovering the amplitude of a PMF of  $B_{1 \text{ Mpc}} = 1.08 \text{ nG}$ . This amplitude is within the 95% C.L. limits from current CMB measurements as Planck [39] and Planck+SPT [25] (see [55, 56] for constraints on pre-Planck data with the same methodology).

The constraints on  $B_{1 \text{ Mpc}}$  from our selection of future

experiments are reported in Tab. IV. In the first row we report the results from our analysis without variation in time ratio (fixing it at the value of  $12^6$ ). In this case large satellite experiments as PIXIE and LiteBIRD can recover  $B_{1 \text{ Mpc}}$  with a very good precision of about  $\sigma(B_{1 \text{ Mpc}}) \sim 0.06\text{-}0.03 \text{ nG}$ . Conversely, a satellite mission as CORE-M5, with improved angular resolution respect to PIXIE or LiteBIRD, would measure the PMF amplitude with an excellent accuracy of  $\sigma(B_{1 \text{ Mpc}}) \sim 0.02 \text{ nG}$ . The same accuracy can be achieved by the CMB-S4 experiment. However it is important to note that we assumed a, quite optimistic, value of  $\ell_{\min} = 5$  for CMB-S4. It may be possible that the final  $\ell_{\min}$  will shift towards higher values given a more limited scanning strategy due to, for example, shorter observation time and high frequency foregrounds. The Stage-3 experiment in both configurations “wide” or “deep” will provide much weaker constraints. This is due to the fact that the large angular scale  $B$ -mode is sampled with less accuracy by the Stage-3 experiment.

It is interesting to note that while experiments as CORE-M5 and CMB-S4 can bound a PMF with amplitude of  $B_{1 \text{ Mpc}} = 1.08 \text{ nG}$  with a  $\sigma(B_{1 \text{ Mpc}}) \sim 0.02 \text{ nG}$  precision, the upper limit on  $B_{1 \text{ Mpc}}$  achievable from CMB-S4 in case of no PMF is  $B_{1 \text{ Mpc}} < 0.52 \text{ nG}$  at 68% C.L. (see e.g. [29]). This is due to the fact that the amplitude of the  $B$ -mode polarization from PMF scales as  $C_\ell \sim B_{1 \text{ Mpc}}^4$ . This means that the CMB will be able to highly constrain a PMF, if detected, but also that upper limits on  $B_{1 \text{ Mpc}}$  will be only marginally improved by future experiments (by a factor four in case of CMB-S4 if we compare with the upper limit of  $2 \text{ nG}$  from Planck).

These constraints are obtained under the assumption of a perfect knowledge of the time ratio and this is obviously not a realistic case. As we see from the second row of Tab. IV, letting also this parameter free to vary weakens the constraints on  $B_{1 \text{ Mpc}}$ . The constraints on  $B_{1 \text{ Mpc}}$  are relaxed by a factor  $\sim 4\text{-}5$  for the PIXIE and LiteBIRD experiments, a factor  $\sim 2$  for CORE-M5 and by  $\sim 50\%$  for CMB-S4. Moreover, the time ratio is bounded essentially just with the CORE-M5 and CMB-S4 experiments.

Let us now move to investigate a possible degeneracy with a primordial GW component. To this goal, we perform three different additional analyses on a fiducial model with  $B_{1 \text{ Mpc}} = 1.08 \text{ nG}$  and  $r = 0$ :

- In the first analysis we wrongly assume no PMF and we let to vary only  $r$  with a tensor spectral index  $n_t$  given by the inflationary consistency relation  $n_t = -r/8$ . In this run we therefore quantify how the assumption of no PMF could bias the determination of  $r$  and therefore provide a misleading first detection of primordial gravitational waves.

<sup>6</sup> This choice will lead to constraint the minimum value of the amplitude  $B_{1 \text{ Mpc}}$  in the scheme we outlined in section II.

- In the second analysis we consider as free parameters both  $r$  and a  $B_{1\text{Mpc}}$  but again we fix the ratio  $\eta_\nu/\eta_B$ . This run is therefore useful to understand if a CMB experiment could discriminate between inflationary GWs and a PMF when the latter is described just by one single parameter.
- In the third analysis we vary  $r$ ,  $B_{1\text{Mpc}}$  and  $\eta_\nu/\eta_B$ . As noticed in [29], since the time ratio determines the amplitude of the passive tensor modes, it is mostly degenerate with  $r$  in the  $B$ -mode polarization.

The results of these three analysis are reported in Tab. V. As we can see from the first row of Tab. V, analyzing a CMB dataset with the wrong assumption of no PMF and  $B_{1\text{Mpc}} = 0$  could lead to a bias on the tensor-to-scalar ratio  $r$ . An experiment as PIXIE could provide an indication at above three standard deviations for a primordial tensor amplitude of  $r \sim 0.0065$ . LiteBIRD, CORE-M5 and CMB-S4 will provide an evidence for  $r > 0$  even higher, with statistical significances that could reach (and also go over) about 10 standard deviations. Again, we like to point out that we have  $r = 0$  and no inflationary tensor modes in our fiducial model. The experimental evidence for  $r > 0$  that these experiments obtain is therefore completely misleading and based on the wrong assumption of  $B_{1\text{Mpc}} = 0$ .

The next step consists in letting also  $B_{1\text{Mpc}}$  to vary and see if these future experiments will be able to discriminate between  $r$  and  $B_{1\text{Mpc}}$ . The results of this analysis are on the second row of Tab. V. As we can see, when  $B_{1\text{Mpc}}$  is included, the detection for  $r > 0$  simply disappears or is rather weaker for PIXIE, LiteBIRD and Stage-3 experiments. However, for these experiments, there is also no clear detection for  $B_{1\text{Mpc}}$ . What is happening is clear by looking at Figure 3: a clear degeneracy is present on the  $B_{1\text{Mpc}}$  vs.  $r$  plane and the experiments are simply unable to discriminate between a genuine primordial tensor component from gravitational waves and a PMF. For PIXIE and LiteBIRD this is essentially due to the poor experimental angular resolution that does not allow to access small scales,  $\ell \gtrsim 1000$ , where the vector compensated PMF  $B$ -mode could be detected. Indeed, when we consider experiments with better angular resolution as CORE-M5 and CMB-S4 the degeneracy is broken, the PMF is well measured and just an upper limit is obtained for  $r$ . For the Stage-3 experiment a degeneracy between  $r$  and  $B_{1\text{Mpc}}$  is also present: this is essentially due to the lower experimental sensitivity that does not allow clear detection of the  $B$ -mode signal of the fiducial model.

## B. Delensing

In this section we briefly study the impact of delensing on the forecasted constraints in the  $B_{1\text{Mpc}}$  vs.  $r$  plane from the simulated data for LiteBIRD, CMB-S4

and CORE-M5, using the likelihood of Eq. (20) and fixing all parameters apart from  $r$  and  $B_{1\text{Mpc}}$ . The values of the delensing parameter  $\alpha$  are listed in Tab. III. To obtain the “t+PMF” angular spectra of Eq. (21) we rescale two templates computed for  $r = 0.1, B_{1\text{Mpc}} = 0\text{ nG}$  and  $r = 0, B_{1\text{Mpc}} = 1.08\text{ nG}$ . We leave  $n_t$  fixed to  $-0.1/8$ , even if  $r$  is varied: at such low values of  $r$  as those probed by LiteBIRD, CMB-S4 and CORE-M5 the error is negligible (this is confirmed a posteriori by comparing Fig. 4 with Fig. 3).

The 68% C.L. and 95% C.L. contours are reported in Fig. 4. First, we notice that even fixing all parameters apart from  $B_{1\text{Mpc}}$  and  $r$  leads to only marginally more stringent constraints than those depicted in Fig. 3. Most importantly, we also see that delensing will not help to break the degeneracy between the two parameters for LiteBIRD. For CORE-M5 and CMB-S4, instead, delensing would shrink the 95% C.L. contours of roughly a factor of 2.

We did not show the forecasts for Stage-3 or PIXIE in Fig. 4: as for LiteBIRD, also in this case delensing would not help in breaking the degeneracy between  $r$  and  $B_{1\text{Mpc}}$ .

## C. Importance of small-scale $B$ -mode measurements

Finally, we investigate in more detail the differences between LiteBIRD and CMB-S4.

We consider two different models with roughly the same  $\chi_{\text{min}}^2$  for the LiteBIRD simulated dataset, but with very different values of  $r$  and  $B_{1\text{Mpc}}$ : the model “(1)” has ( $r = 1.76 \times 10^{-5}, B_{1\text{Mpc}} = 1.064\text{ nG}$ ), while the model “(2)” has ( $r = 7.22 \times 10^{-3}, B_{1\text{Mpc}} = 7.57 \times 10^{-2}\text{ nG}$ ). Then, we expect that for LiteBIRD it will be impossible to distinguish between these two models, while CMB-S4 will be able to break the degeneracy between them.

We can estimate how well the two experiments are able to distinguish model (2) from model (1) by constructing a simple  $\chi_\ell^2 \equiv (\Delta C_\ell/\sigma_\ell)^2$  for the difference  $\Delta C_\ell \equiv C_\ell^{(2)} - C_\ell^{(1)}$ . Thus, assuming uncorrelated multipoles, we can write the cumulative signal-to-noise ratio ( $S/N$ ) as

$$(S/N)_{\ell_{\text{max}}}^2 = \sum_{\ell=2}^{\ell_{\text{max}}} \frac{\left(C_\ell^{(2)} - C_\ell^{(1)}\right)^2}{\sigma_\ell^2}, \quad (23)$$

where we focus on  $B$ -modes only and  $\sigma_\ell$  is given by noise plus cosmic variance, i.e. [57]

$$\sigma_\ell = \sqrt{\frac{2}{(2\ell+1)f_{\text{sky}}}} \left(C_\ell^{(1)} + N_\ell\right). \quad (24)$$

We plot  $S/N$  for varying  $\ell_{\text{max}}$  in Fig. 5: we see that for LiteBIRD the cumulative signal-to-noise ratio remains of order 1 up to high  $\ell_{\text{max}}$ , while for CMB-S4 it becomes of order 10 at  $\ell_{\text{max}} \gtrsim 1000$ .

	PIXIE	LiteBIRD	CORE-M5	Stage-3 (Deep)	Stage-3 (Wide)	CMB-S4
$\log_{10}(\eta_\nu/\eta_B) = 12$						
$B_{1\text{ Mpc}}$ (nG)	$1.074 \pm 0.055$	$1.078^{+0.034}_{-0.028}$	$1.080 \pm 0.019$	$0.86^{+0.41}_{-0.13}$	$0.902^{+0.35}_{-0.098}$	$1.079 \pm 0.020$
$\log_{10}(\eta_\nu/\eta_B)$ free						
$B_{1\text{ Mpc}}$ (nG)	$1.16^{+0.15}_{-0.24}$	$1.15^{+0.12}_{-0.24}$	$1.066^{+0.064}_{-0.049}$	$0.89^{+0.41}_{-0.17}$	$0.87^{+0.45}_{-0.18}$	$1.074 \pm 0.032$
$\log_{10}(\eta_\nu/\eta_B)$	unconstrained	unconstrained	$12.39^{+0.98}_{-1.7}$	unconstrained	$11.4^{+2.9}_{-4.0}$	$12.16^{+0.81}_{-0.97}$

Table IV. 68% C.L. constraints on  $B_{1\text{ Mpc}}$  and  $\log_{10}(\eta_\nu/\eta_B)$  for the experiments listed in Tab. I. These runs are realized assuming no gravitational waves in the MCMC analysis *i.e.* we have  $r = 0$ .

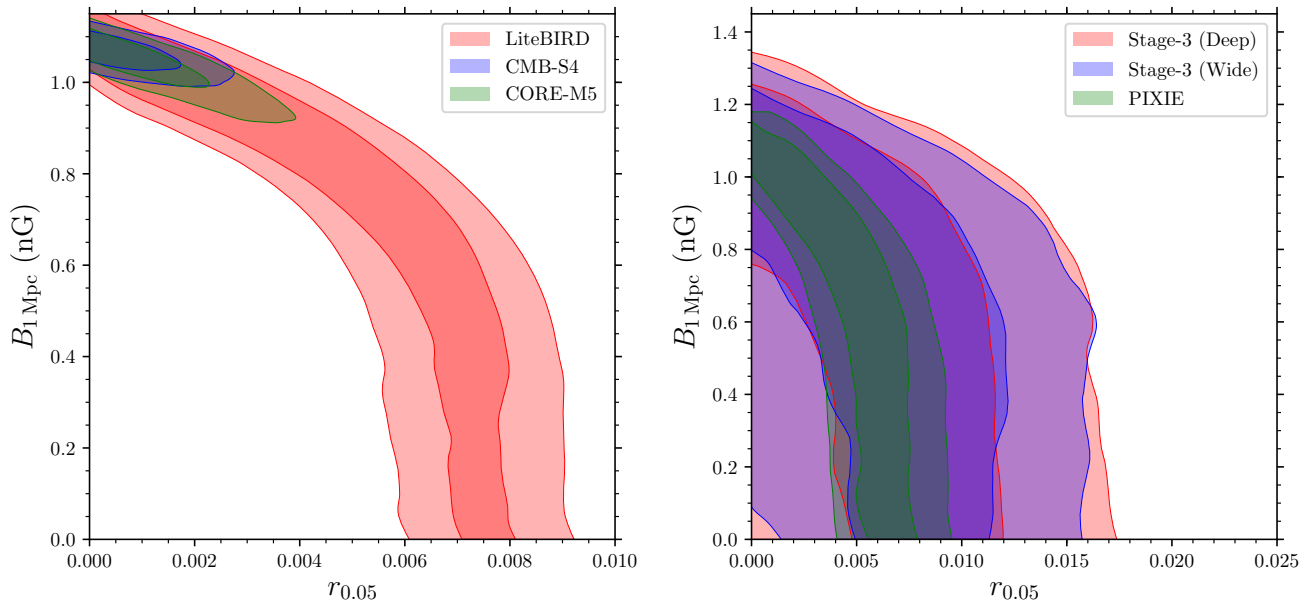


Figure 3. Forecasted constraints on the  $B_{1\text{ Mpc}}$  vs.  $r$  plane from MCMC analyses on simulated CMB angular spectra data for LiteBIRD and CMB-S4 (Left Panel) and for PIXIE, Stage-3, and CORE-M5 (Right Panel). The fiducial model has  $B_{1\text{ Mpc}} = 1.08\text{ nG}$  and  $r = 0$ . Clearly the LiteBIRD, PIXIE and Stage-3 experiments are unable to distinguish the PMF from inflationary gravitational waves. On the contrary, CMB-S4 and CORE-M5 can break the degeneracy thanks to better sensitivity to small scale  $B$ -modes.

	PIXIE	LiteBIRD	CORE-M5	Stage-3 (Deep)	Stage-3 (Wide)	CMB-S4
$r$	$0.0065^{+0.0013}_{-0.0015}$	$0.00733 \pm 0.00088$	$0.00725 \pm 0.00056$	$0.0084^{+0.0039}_{-0.0052}$	$0.0084^{+0.0038}_{-0.0046}$	$0.00717 \pm 0.00072$
$r$	$0.0050^{+0.0028}_{-0.0019}$	$0.0050^{+0.0034}_{-0.0041}$	$< 0.00149$	$0.0070^{+0.0027}_{-0.0061}$	$0.0071^{+0.0032}_{-0.0057}$	$< 0.00112$
$B_{1\text{ Mpc}}$ (nG)	$0.59^{+0.45}_{-0.27}$	$0.66^{+0.45}_{-0.22}$	$1.034^{+0.052}_{-0.027}$	$0.60 \pm 0.34$	$0.59^{+0.40}_{-0.36}$	$1.058^{+0.030}_{-0.024}$
$r$	$0.0049^{+0.0027}_{-0.0019}$	$0.0051^{+0.0033}_{-0.0018}$	$0.0029^{+0.0014}_{-0.0024}$	$0.0074^{+0.0032}_{-0.0060}$	$0.0071^{+0.0034}_{-0.0052}$	$0.0031 \pm 0.0017$
$B_{1\text{ Mpc}}$ (nG)	$< 0.847$	$0.70^{+0.44}_{-0.36}$	$1.057^{+0.065}_{-0.0482}$	$< 0.820$	$0.62^{+0.35}_{-0.53}$	$1.073^{+0.037}_{-0.031}$
$\log_{10}(\eta_\nu/\eta_B)$	unconstrained	unconstrained	$9.7^{+1.9}_{-2.5}$	unconstrained	$< 12.7$	$9.3 \pm 1.8$

Table V. 68% C.L. constraints on  $B_{1\text{ Mpc}}$ ,  $\log_{10}(\eta_\nu/\eta_B)$  and  $r$  for the experiments listed in Tab. I.

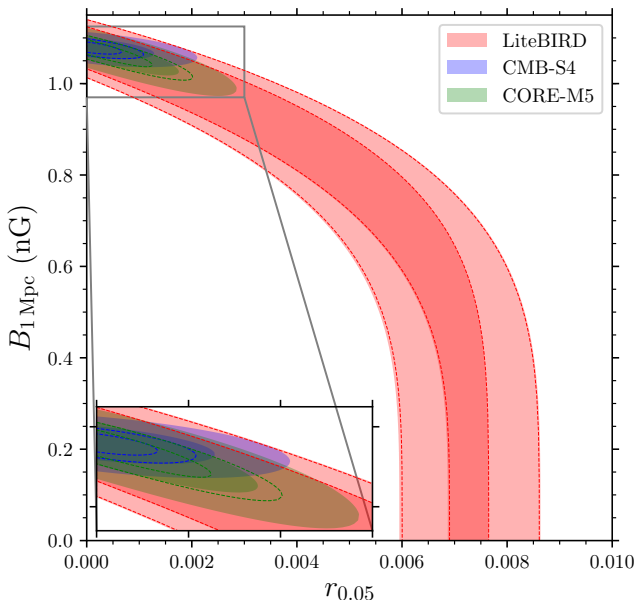


Figure 4. Forecasts in the  $B_{1\text{Mpc}}$  vs.  $r$  plane for LiteBIRD, CMB-S4 and CORE-M5, using the likelihood of Eq. (20). Dashed lines represent the 68% C.L. and 95% C.L. contours after delensing. Clearly, the delensing procedure affects the constraints on  $r$  and  $B_{1\text{Mpc}}$  only if the degeneracy between the two is broken.

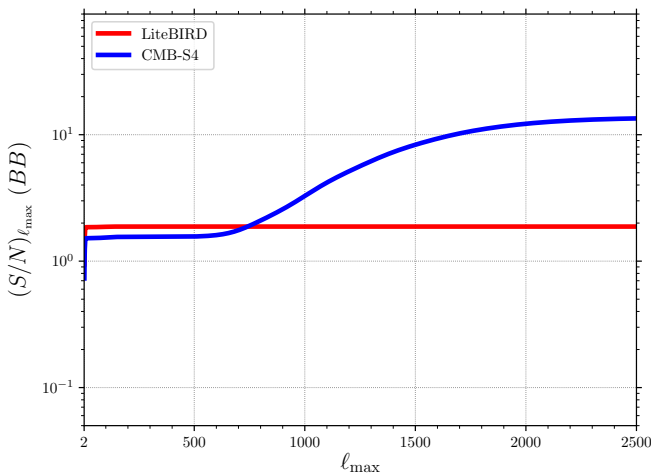


Figure 5. Signal-to-noise ratio for varying  $\ell_{\text{max}}$  of Eq. (23) for the LiteBIRD and CMB-S4 experiments.

We can show the importance of including small angular scales in a different way by using directly the full  $B$ -mode likelihood for the CMB-S4 experiment, as we did in our analysis of the impact of delensing. Varying  $\ell_{\text{max}}$  in the

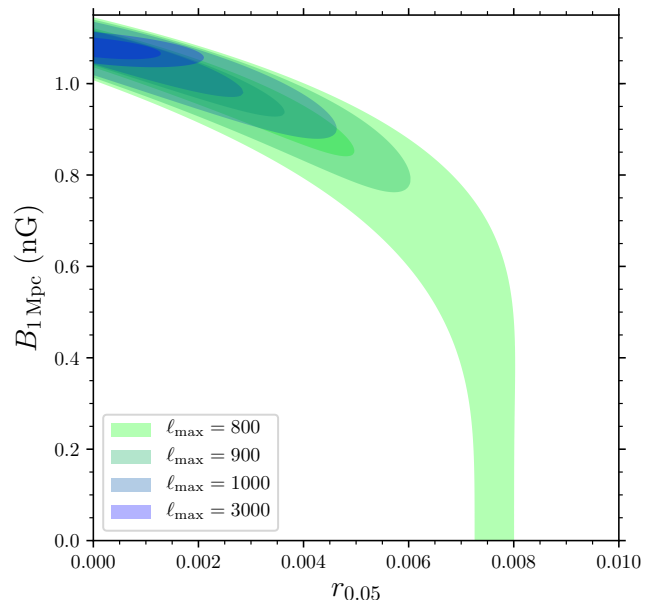


Figure 6. Impact of varying  $\ell_{\text{max}}$  on CMB-S4 constraints: we see that the degeneracy between  $r$  and  $B_{1\text{Mpc}}$  is broken if  $B$ -mode anisotropies can be measured on scales  $\ell \gtrsim 900$

sum over  $\ell$  of Eq. (20),<sup>7</sup> we can see at which angular scale the degeneracy between  $r$  and  $B_{1\text{Mpc}}$  can be broken by this experiment. In Fig. 6, we see that this happens at  $\ell_{\text{max}} \gtrsim 900$ : if CMB-S4 could not access higher multipoles, the constraints on  $r$  and  $B_{1\text{Mpc}}$  would be similar to those of LiteBIRD.

## V. CONSTRAINTS FROM FARADAY ROTATION

PMFs also induce Faraday rotation (FR) of CMB polarization. It is therefore useful to evaluate the ability of future CMB experiments to detect a PMF with an amplitude of 1.08 nG through FR and break the possible degeneracies between  $r$  and  $B_{1\text{Mpc}}$ .

FR of the linear polarization of CMB photons is described by the rotation angle  $\alpha_F$ , defined in terms of the Stokes  $Q$  and  $U$  parameters by  $(Q \pm iU)(\hat{n}) \rightarrow (Q \pm iU)(\hat{n})e^{\pm 2i\alpha(\hat{n})}$ . An inhomogeneous magnetic field sources anisotropies in the rotation angle, whose angular power spectrum will be related to the two-point correlation function of the magnetic field as given in Eqs. (5), (6) (see, e.g., [58–61]). The angular power spectrum  $C_\ell^{\alpha_F \alpha_F}$  of the rotation angle  $\alpha_F(\hat{n})$  can be constrained directly by exploiting the fact that, at first order in  $\alpha_F$ , the off-diagonal elements of the two-point correlation functions of  $E$ - and  $B$ -modes are proportional to the rotation

<sup>7</sup> Fixing the delensing parameter  $\alpha$  to 0.

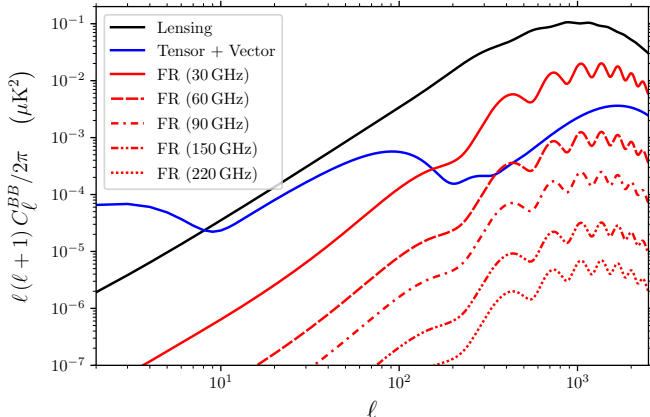


Figure 7.  $B$ -modes angular spectrum from Faraday rotation (1.08 nG magnetic field amplitude is assumed) at frequencies of 30 GHz, 60 GHz, 90 GHz, 150 GHz and 220 GHz. Also  $B$ -modes from magnetic perturbations are shown, together with the standard lensing predictions. Clearly the  $B$ -modes from Faraday rotation are completely negligible for an experiment mostly sensitive to frequencies around 150 GHz as those considered in this paper. PIXIE will operate also at lower frequencies but at very low multipoles, where the Faraday rotation signal will be anyway negligible.

field [62].<sup>8</sup> One can take advantage of this feature to build a quadratic estimator to measure the anisotropic rotation [62–64]. The rotation of  $E$ -modes into  $B$ -modes, moreover, leads to a contribution  $C_\ell^{BB,FR}$  that should be in principle added to Eq. (15). However the angular spectrum  $C_\ell^{\alpha_F\alpha_F}$ , and then  $C_\ell^{BB,FR}$ , scales as  $\nu^{-4}$ : thus we expect to have a larger signal for these FR-induced  $B$ -modes at lower frequencies (e.g.  $\nu \sim 30$  GHz), that will not be optimally sampled by the experiments considered here. Indeed, these experiments are not conceived for a measurement at these frequencies for mainly two reasons:

- lower frequencies are more contaminated by galactic foregrounds and are mostly used to identify and remove them rather than to extract genuine cosmological information;
- for a given experimental configuration, lower frequencies are limited by diffraction and have smaller angular resolution. Therefore, space experiments such as CORE-M5 or LiteBIRD have been designed with the largest number of detectors at frequencies around  $\sim 150$  GHz where the minimal foreground contamination is expected.

<sup>8</sup> Working in the flat-sky approximation, one has  $\langle E^*(\ell)B(\ell') \rangle \rightarrow \langle E^*(\ell)B(\ell') \rangle + f_{EB}(\ell, \ell')\alpha(\ell - \ell')$ , where the matrix  $f_{EB}$  is constructed from the  $EE$  and  $BB$  angular power spectra [62].

In Fig. 7 we plot the expected signal in the  $B$ -mode angular power spectrum from Faraday rotation generated by a magnetic field of 1.08 nG for various frequencies. The Faraday rotation  $B$ -modes are obtained using Eq. (38) of [58]. In Fig. 7 we also plot the lensing  $B$ -mode spectrum and the frequency-independent contribution of Eq. (15), i.e. the one generated by vector- and tensor-mode perturbations in the metric, sourced by the stress-energy in the PMF. As we can clearly see, the  $B$ -modes from Faraday rotation at 150 GHz are about four orders of magnitude smaller than the lensing signal, i.e. they will be undetectable by an experiment operating at those frequencies. At 30 GHz the signal is much larger, however none of the experiment considered in this paper will sample this frequency with the exception of PIXIE. In this case, however, the angular resolution will not be sufficient to detect the  $B$ -modes from Faraday rotation, since PIXIE can arrive at most at  $l_{\max} = 500$ .

The LiteBIRD and CORE-M5 could produce full CMB sky maps at frequencies of 60 GHz. It is therefore interesting to investigate if these  $B$ -modes from FR could be detected by these experiments. Unfortunately, as we show in Fig. 8, neither of these two experiments will be able to detect them. Indeed, they will not have enough sensitivity and angular resolution at these frequencies.

To summarize, the contribution  $C_\ell^{BB,FR}$  to the  $B$ -mode angular power spectrum induced by a PMF of 1.08 nG is not detectable by the experiments considered here. For this reason, in the following we will focus on a forecast for the detection of anisotropies in the FR angle  $\alpha_F$  of the  $E$  modes: clearly, a detection of  $\alpha_F$  would allow to confirm whether an eventual  $B$ -mode measurement is due to primordial GWs or to PMFs.

Then, in order to perform this kind of forecast we consider the following approximated angular power spectrum in the fluctuations of the rotation angle  $\alpha_F$  induced by a nearly scale-invariant PMF of 1.08 nG (see e.g. Eq. (4) in [61]):

$$\frac{L(L+1)C_L^{\alpha_F\alpha_F}}{2\pi} = 4.2 \times 10^{-8} \text{ rad}^2, \quad (25)$$

where we have assumed a CMB observational frequency of  $\nu \sim 150$  GHz. We have then estimated the experimental noise on  $C_L^{\alpha_F\alpha_F}$  and computed the relevant signal to noise ratio  $S/N$  using the quadratic estimator described in [63, 64] (see Appendix A). For simplicity we have neglected the contamination of “spurious” FR induced by magnetic fields in our galaxy and lensing. Our results should therefore be considered as optimistic since the removal of these terms could lead to a significantly lower  $S/N$  (see [29]). The results of our analysis are reported in Tab. VI.

As we can see from Tab. VI, experiments as PIXIE and LiteBIRD will be essentially unable to detect our fiducial PMF through FR. This is mainly due to the poor angular resolution that does not let these experiments measure  $E$ - and  $B$ -modes at  $\ell \sim 1000$ , i.e. at scales that are relevant for a measure of  $\alpha_F$ . Including the frequency dependence

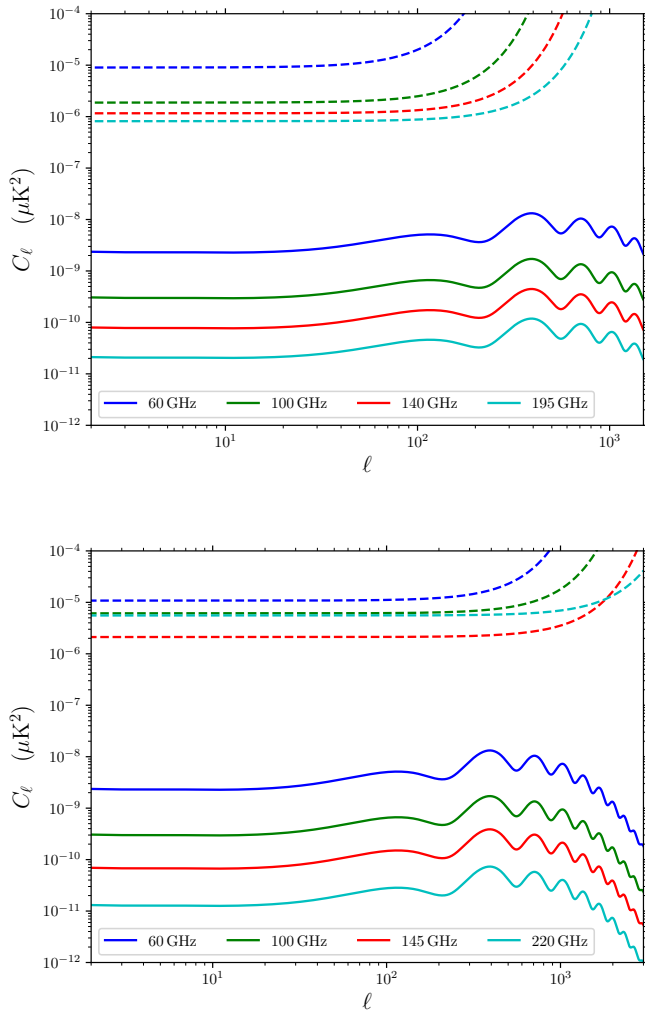


Figure 8. Expected experimental white noise for the lowest channels of LiteBIRD (top panel) and CORE-M5 (bottom panel), together with the expected signal from  $B$ -modes generated by Faraday rotation (for a PMF of 1.08 nG) at the same frequencies. Clearly, the signal is undetectable in any frequency channel by both experiments.

Experiment	$S/N$
PIXIE	0.05
LiteBIRD	0.7
CORE-M5	15
Stage-3 (Deep)	20
Stage-3 (Wide)	2
CMB-S4	$10^2$

Table VI.  $S/N$  ratio for the detection of a nearly scale-invariant PMF of 1.08 nG through Faraday rotation for different experimental configurations. The values are obtained using a quadratic estimator as in [63, 64]. We neglect galactic foregrounds and lensing.

of the signal will not change this result since at lower frequencies would correspond also an even lower angular resolution. On the contrary, the Stage-3 experiment, especially in the “deep” configuration, will be able to detect the PMF via FR with high accuracy. While in this case  $r$  is poorly constrained, a combination with the LiteBIRD experiment could be extremely important. The CMB-S4 experiment will constrain a PMF with great accuracy, in agreement with the results presented in [29].

## VI. CONCLUSIONS

PMFs are a fascinating subject still under active investigation. In the past years it has been made clear by several authors that PMFs can leave characteristic imprints on the CMB angular power spectrum. The Planck collaboration already reported stringent constraints and future experiments will improve them. In this paper we investigated the impact that a PMF with an amplitude of  $\sim 1$  nG, compatible with current CMB limits, could have in the search of primordial gravitational waves generated during inflation. What we have found is that for satellite missions as PIXIE or LiteBIRD that are limited to large angular scales, a degeneracy is present between  $B_{1\text{Mpc}}$  and  $r$  that would not let these experiments to determine the true nature of the observed  $B$ -mode. What is needed is a better angular resolution as planned in the CORE-M5 proposal or the CMB-S4 experiment. This could let a measurement of the small scale  $B$ -mode discriminating signal from PMF vector compensated perturbations.

Another possibility is to detect PMF through Faraday rotation of the CMB polarization. While  $B$  modes induced by FR are practically undetectable by the experiments considered here, a better opportunity is offered by measurements of anisotropies in the FR angle.

While also in this case PIXIE and LiteBIRD will not be able to significantly detect the PMF, we have found that the Stage-3 experiment could already put stringent constraints on it. A nice complementarity therefore exists between the LiteBIRD and Stage-3 experiments that could let to break the  $r$  vs.  $B_{1\text{Mpc}}$  degeneracy.

Before concluding it is important to note that PMF of the order of  $\sim 1$  nG are already not compatible when the ionization history of the Universe is considered (see [39]) that places an upper limit of 0.90 nG at 95% C.L. PMFs are indeed damped on small scales, leading to heating of baryons and electrons and producing Compton- $\gamma$  distortions in the CMB. However uncertainties in the modeling of the heating and in the reionization process may affect the constraint [65]. Moreover, a PMF field of  $\sim 0.9$  nG would produce a  $B$ -mode spectrum essentially rescaled by a factor of 0.48 with respect to the one considered here. This could still bias future CMB polarization searches for primordial gravitational waves.

It is also worthwhile to mention that bispectrum and trispectrum measurements could also place strong constraints on magnetic fields [39, 66, 67].

In summary, PMFs can affect future CMB constraints on primordial gravitational waves and our study reinforces the importance of future experimental constraints on PMFs. Future constraints at the level of 0.2 nG, as expected from FR measurements by the CMB-S4 experiment (see also [29]), will be crucial in limiting a spurious  $B$ -mode PMF contribution to sub-percent level respect to the value of  $r \sim 0.005$  expected by the Starobinski model.

## ACKNOWLEDGMENTS

We are clearly indebted to Levon Pogosian and Alex Zucca for providing their MAGCAMB code and for useful comments. We thank Antony Lewis for providing his CosmoMC code. It is also a pleasure to thank Robert Caldwell, Ruth Durrer, Franz Elsner, and Takeshi Kobayashi for extremely useful comments and suggestions. EDV acknowledges support from the European Research Council in the form of a Consolidator Grant with number 681431.

- 
- [1] M. Kamionkowski and E. D. Kovetz, *Ann. Rev. Astron. Astrophys.* **54** (2016) 227 [[arXiv:1510.06042](#) [astro-ph.CO]].
- [2] D. Baumann, [arXiv:0907.5424](#) [hep-th].
- [3] M. C. Guzzetti, N. Bartolo, M. Liguori and S. Matarrese, *Riv. Nuovo Cim.* **39** (2016) no.9, 399 [[arXiv:1605.01615](#) [astro-ph.CO]].
- [4] L. Senatore, [arXiv:1609.00716](#) [hep-th].
- [5] H. C. Chiang *et al.*, *Astrophys.J.* **711**:1123-1140,2010
- [6] P. A. R. Ade *et al.* [BICEP2 and Keck Array Collaborations], *Phys. Rev. Lett.* **116** (2016) 031302 [[arXiv:1510.09217](#) [astro-ph.CO]].
- [7] G. Cabass, L. Pagano, L. Salvati, M. Gerbino, E. Giusarma and A. Melchiorri, *Phys. Rev. D* **93** (2016) no.6, 063508 [[arXiv:1511.05146](#) [astro-ph.CO]].
- [8] J. A. Grayson *et al.* [BICEP3 Collaboration], *Proc. SPIE Int. Soc. Opt. Eng.* **9914** (2016) 99140S [[arXiv:1607.04668](#) [astro-ph.IM]].
- [9] T. Essinger-Hileman *et al.*, Society of Photo-Optical Instrumentation Engineers (SPIE) Conference Series, vol. 9153 of Society of Photo-Optical Instrumentation Engineers (SPIE) Conference Series, p. 1, July, 2014. [arXiv:1408.4788](#).
- [10] S. W. Henderson *et al.*, *J. Low. Temp. Phys.* **184** (2016) no.3-4, 772 [[arXiv:1510.02809](#) [astro-ph.IM]].
- [11] B. A. Benson *et al.*, Society of Photo-Optical Instrumentation Engineers (SPIE) Conference Series, vol. 9153 of Society of Photo-Optical Instrumentation Engineers (SPIE) Conference Series, p. 1, July, 2014. [arXiv:1407.2973](#).
- [12] A. Suzuki *et al.*, [[arXiv:1801.06987](#) [astro-ph.IM]].
- [13] E. Di Valentino *et al.* [CORE Collaboration], [arXiv:1612.00021](#) [astro-ph.CO].
- [14] F. Finelli *et al.* [CORE Collaboration], [arXiv:1612.08270](#) [astro-ph.CO].
- [15] J. Delabrouille *et al.* [CORE Collaboration], [arXiv:1706.04516](#) [astro-ph.IM].
- [16] K. N. Abazajian *et al.* [CMB-S4 Collaboration], [arXiv:1610.02743](#) [astro-ph.CO].
- [17] J. Errard, S. M. Feeney, H. V. Peiris and A. H. Jaffe, *JCAP* **1603** (2016) no.03, 052 [[arXiv:1509.06770](#) [astro-ph.CO]].
- [18] M. Remazeilles *et al.* [CORE Collaboration], [arXiv:1704.04501](#) [astro-ph.CO].
- [19] J. Lizarraga, J. Urrestilla, D. Daverio, M. Hindmarsh, M. Kunz and A. R. Liddle, *Phys. Rev. Lett.* **112** (2014) 171301 [[arXiv:1403.4924](#) [astro-ph.CO]].
- [20] A. Moss and L. Pogosian, *Phys. Rev. Lett.* **112** (2014) 171302 [[arXiv:1403.6105](#) [astro-ph.CO]].
- [21] C. Bonvin, R. Durrer and R. Maartens, *Phys. Rev. Lett.* **112** (2014) no.19, 191303 [[arXiv:1403.6768](#) [astro-ph.CO]].
- [22] F. Finelli, F. Paci and D. Paoletti, *Phys. Rev. D* **78** (2008) 023510 [[arXiv:0803.1246](#) [astro-ph]].
- [23] D. Paoletti, F. Finelli and F. Paci, *Mon. Not. Roy. Astron. Soc.* **396** (2009) 523 [[arXiv:0811.0230](#) [astro-ph]].
- [24] J. R. Shaw and A. Lewis, *Phys. Rev. D.* **81** (2010) 043517 [[arXiv:0911.2714](#) [astro-ph.CO]].
- [25] A. Zucca, Y. Li and L. Pogosian, *Phys. Rev. D* **95** (2017) no.6, 063506 [[arXiv:1611.00757](#) [astro-ph.CO]].
- [26] S. Camera, C. Fedeli and L. Moscardini, *JCAP* **03** (2014) 027 [[arXiv:1311.6383](#) [astro-ph.CO]].
- [27] D. R. Sutton, C. Feng and C. L. Reichardt, *Astrophys. J.* **846** (2017) no.2, 164 [[arXiv:1702.01871](#) [astro-ph.CO]].
- [28] R. Durrer and A. Neronov, *A.&ARv.* **21** (2013) 62 [[arXiv:1303.7121](#) [astro-ph.CO]].
- [29] L. Pogosian and A. Zucca, [arXiv:1801.08936](#) [astro-ph.CO].
- [30] K. Subramanian, *Rep. Prog. Phys.* **79** (2016) 076901 [[arXiv:1504.02311](#) [astro-ph.CO]].
- [31] D. Grasso and H. R. Rubinstein, *Phys. Rep.* **348** (2001) 163 [[astro-ph/0009061](#) [astro-ph.CO]].
- [32] C. Bonvin, C. Caprini and R. Durrer, *Phys. Rev. D.* **88** (2013) 083515 [[arXiv:1308.3348](#) [astro-ph.CO]].
- [33] T. Kobayashi *JCAP* **05** (2014) 040 [[arXiv:1403.5168](#) [astro-ph.CO]].
- [34] D. Green and T. Kobayashi *JCAP* **03** (2016) 010 [[arXiv:1511.08793](#) [astro-ph.CO]].
- [35] T. Kobayashi and N. Afshordi, *JHEP* **1410**, 166 (2014) [[arXiv:1408.4141](#) [hep-th]].
- [36] A. Lewis, *Phys. Rev. D.* **70** (2004) 043011 [[astro-ph/0406096](#)].
- [37] K. Kojima, T. Kajino and G. J. Mathews *JCAP* **1002** (2010) 018 [[arXiv:0910.1976](#) [astro-ph.CO]].
- [38] C. Caprini and R. Durrer, *Phys. Rev.* **D65** (2001) 023517 [[astro-ph/0106244](#)].
- [39] P. A. R. Ade *et al.* [Planck Collaboration], *Astron. Astrophys.* **594** (2016) A19 [[arXiv:1502.01594](#) [astro-ph.CO]].
- [40] A. Mack, T. Kahniashvili, A. Kosowsky *Phys. Rev.* **D65** (2001) 123004
- [41] K. Subramanian and J. D. Barrow, *Phys. Rev. Lett.* **81** (1998) 3575 [[astro-ph/9803261](#)].
- [42] L. Perotto, J. Lesgourgues, S. Hannestad, H. Tu and Y. Y. Y. Wong, *JCAP* **0610**, 013 (2006).

- [43] A. Kogut et al., *Journal of Cosmology and Astroparticle Physics*, Issue 07, id. 025 (2011).
- [44] R. Allison, P. Caucal, E. Calabrese, J. Dunkley and T. Louis, *Phys. Rev. D* **92** (2015) no.12, 123535 [[arXiv:1509.07471](#) [astro-ph.CO]].
- [45] A. Lewis, A. Challinor and A. Lasenby, *Astrophys. J.* **538** (2000) 473 [[astro-ph/9911177](#)].
- [46] A. Lewis and S. Bridle, *Phys. Rev. D* **66**, 103511 (2002) [[astro-ph/0205436](#)].
- [47] P. A. R. Ade *et al.* [Planck Collaboration], [[arXiv:1502.01589](#) [astro-ph.CO]].
- [48] N. Aghanim *et al.* [Planck Collaboration], *Astron. Astrophys.* **596** (2016) A107 [[arXiv:1605.02985](#) [astro-ph.CO]].
- [49] A. A. Starobinsky, *Phys. Lett.* **91B**, 99 (1980).
- [50] R. Kallosh, A. Linde and D. Roest, *JHEP* **1311**, 198 (2013) [[arXiv:1311.0472](#) [hep-th]].
- [51] K. M. Smith, D. Hanson, M. LoVerde, C. M. Hirata and O. Zahn, *JCAP* **1206**, 014 (2012) [[arXiv:1010.0048](#) [astro-ph.CO]].
- [52] J. Errard, S. M. Feeney, H. V. Peiris and A. H. Jaffe, *JCAP* **1603**, no. 03, 052 (2016) [[arXiv:1509.06770](#) [astro-ph.CO]].
- [53] B. D. Sherwin and M. Schmittfull, *Phys. Rev. D* **92**, no. 4, 043005 (2015) [[arXiv:1502.05356](#) [astro-ph.CO]].
- [54] T. Okamoto and W. Hu, *Phys. Rev. D* **67**, 083002 (2003) [[astro-ph/0301031](#)].
- [55] D. Paoletti and F. Finelli, *Phys. Rev. D* **83** (2011) 123533 [[arXiv:1005.0148](#) [astro-ph.CO]].
- [56] D. Paoletti and F. Finelli, *Phys. Lett. B* **726** (2013) 45 [[arXiv:1208.2625](#) [astro-ph.CO]].
- [57] M. Tegmark, *Phys. Rev. D* **56**, 4514 (1997)
- [58] L. Pogosian, A. P. S. Yadav, Y. F. Ng and T. Vachaspati, *Phys. Rev. D* **84** (2011) 043530 Erratum: [*Phys. Rev. D* **84** (2011) 089903] [[arXiv:1106.1438](#) [astro-ph.CO]].
- [59] S. De, L. Pogosian and T. Vachaspati, *Phys. Rev. D* **88** (2013) no.6, 063527 [[arXiv:1305.7225](#) [astro-ph.CO]].
- [60] P. A. R. Ade *et al.* [POLARBEAR Collaboration], *Phys. Rev. D* **92**, 123509 (2015) [[arXiv:1509.02461](#) [astro-ph.CO]].
- [61] P. A. R. Ade *et al.* [BICEP2 and Keck Array Collaborations], *Phys. Rev. D* **96** (2017) no.10, 102003 [[arXiv:1705.02523](#) [astro-ph.CO]].
- [62] A. P. S. Yadav, R. Biswas, M. Su and M. Zaldarriaga, *Phys. Rev. D* **79**, 123009 (2009) [[arXiv:0902.4466](#) [astro-ph.CO]].
- [63] V. Gluscevic, M. Kamionkowski and A. Cooray, *Phys. Rev. D* **80**, 023510 (2009)
- [64] Robert R. Caldwell, Vera Gluscevic, Marc Kamionkowski, *Phys. Rev. D* **84**, 04350 (2011).
- [65] J. Chluba, D. Paoletti, F. Finelli and J. A. Rubiño-Martín, *Mon. Not. Roy. Astron. Soc.* **451** (2015) no.2, 2244 [[arXiv:1503.04827](#) [astro-ph.CO]].
- [66] H. J. Hortua and L. Castaneda, *JCAP* **06** (2017) 020 [[arXiv:1511.02991](#) [astro-ph.CO]].
- [67] P. Trivedi, K. Subramanian and T. R. Seshadri, *Phys. Rev. D* **89** (2014) no.4, 043523 [[arXiv:1312.5308](#) [astro-ph.CO]].